# $^{40}Ca(p,d)^{39}Ca$ reaction at 65 MeV

M. Matoba, O. Iwamoto, Y. Uozumi, and T. Sakae
*Faculty of Engineering, Kyushu University, Fukuoka 812, Japan*

N. Koori
*College of General Education, Tokushima University, Tokushima 770, Japan*

T. Fujiki,* H. Ohgaki,† and H. Ijiri
*Graduate School of Engineering Sciences, Kyushu University, Kasuga 816, Japan*

T. Maki and M. Nakano
*School of Nursing and Technology, University of Occupational and Environmental Health, Kitakyushu 807, Japan*
(Received 29 July 1992)

Cross sections and analyzing powers have been measured for the $^{40}Ca(p,d)^{39}Ca$ reaction with polarized proton beams of 65 MeV incident energy. The data analysis with a standard distorted-wave Born approximation theory provides transferred angular momenta $l$, $j$, and spectroscopic factors for 58 transitions mainly to the $1d_{3/2}$, $2s_{1/2}$, and $1d_{5/2}$ hole states in $^{39}Ca$. The occupation probabilities of the surface shells in $^{40}Ca$ and the spreading widths of the hole states are determined. The damping mechanism of the single hole states is discussed.

PACS number(s): 21.10.Pc, 27.40.+z, 25.40.Hs

## I. INTRODUCTION

The structure of doubly magic nuclei has always supplied examples for severe tests of new concepts in nuclear models, especially of the shell model and related excitations. The excitation of single hole states via one nucleon transfer reactions has broad implications for the single-particle motion in nuclei, and much information has been accumulated. For the same reasons, one nucleon knockout reactions, for example, $(e,e'p)$, $(p,2p)$, and $(p,pn)$ reactions, have been extensively studied. Almost all the investigations up to now were, however, performed with an unpolarized incident beam, except for a few low-lying excited states. Therefore, the assignments of transferred $j$ values have sometimes been ambiguous, and possible polarized beam experiments are desired. The Osaka University AVF cyclotron facility has an excellent experimental possibility with clean polarized proton or deuteron beams and a high-resolution spectrograph. Thus the spectroscopies there are quite interesting. Recently, Chittrakarn *et al.* [1] have reported a measurement of the excitation of a stretched $6^-$ $(\pi f_{7/2}, \nu d_{5/2}^{-1})$ state through the $^{40}Ca(p,n)^{40}Sc$ reaction at 135 MeV and the quenching of the $1d_{5/2}$ hole state in the excitation energy region of 5–10 MeV has an important bearing on the quenching of this stretched state. In this context, pickup data of low resolution (260 keV) taken with a 189 MeV unpolarized proton beam [2] have been referenced. To discuss this problem, it is necessary to remeasure the fragmentation of the $1d_{5/2}$ hole state and to study the properties of the related surface shells in high-resolution experiments.

In the present work, the $^{40}Ca(p,d)^{39}Ca$ reaction was studied at 65 MeV, and the spectra were analyzed to identify levels, assign spin parities, and determine spectroscopic factors of excited hole states in the excitation energy region of 0–9.5 MeV. The data are discussed with concern not only for the characteristics of the $1d_{5/2}$ hole states *vis-á-vis* the excitation of the $6^-$ stretched state, but also for the occupation probability of the surface shells of $^{40}Ca$ and the spreading widths of deeply bound hole states. The experimental procedure and the results are described in Sec. II, the theoretical analysis of the angular distribution is described in Sec. III, the obtained angular momenta and spectroscopic factors are tabulated and discussed in Sec. IV, and the results are summarized in Sec. V. A preliminary report was published in Ref. [3] on the fragmentation of the $1d_{5/2}$ hole state in $^{39}Ca$.

## II. EXPERIMENT

### A. Experimental procedure

The experiment was carried out at the AVF cyclotron facility of the Research Center for Nuclear Physics, Osaka University. A polarized proton beam of 65 MeV energy was momentum analyzed and bombarded a natural calcium target of thickness 1.10 mg/cm$^2$. Emitted deuterons were analyzed with the spectrograph RAIDEN [4] viewed with the focal plane detector system KYUSHU

*Present address: Sony Corporation, Atsugi 243, Japan.
†Present address: Electrotechnical Laboratory, Tsukuba 305, Japan.

 

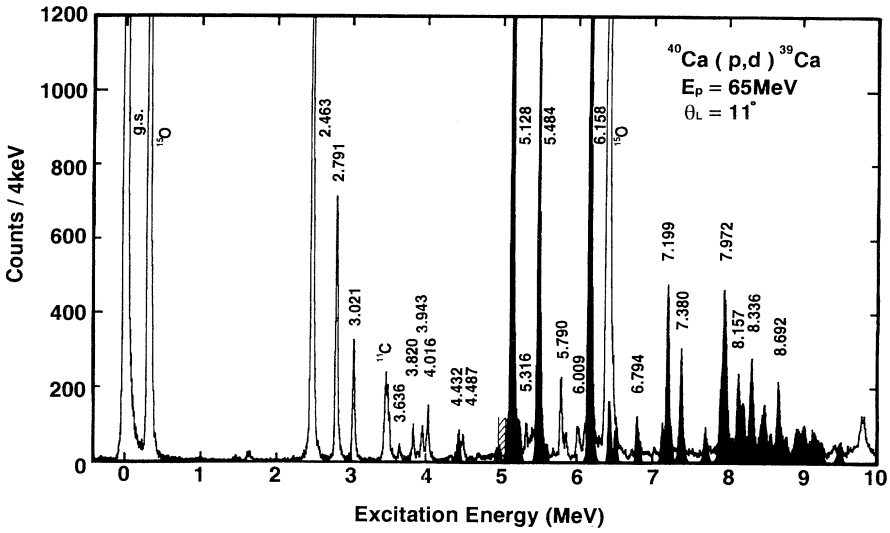


FIG. 1. Typical energy spectrum of deuterons from the $^{40}$Ca$(p,d)^{39}$Ca reaction at 65 MeV. The darkened part corresponds to the $l=2$, $j=\frac{5}{2}$ transitions.

[5]. Angular distributions of cross sections and analyzing powers were measured at 5°–45° laboratory angles. The measured excitation energy region is 0–10 MeV. The normalization of the absolute cross section is performed by scaling the measured $p+{}^{40}$Ca elastic-scattering cross section to an optical-model prediction using parameters of global potentials [6,7]. The accuracy of the normalization is estimated to be better than 10%, which is mainly due to the ambiguity of the procedure for fitting the theoretical to experimental angular distributions. The errors attributed to run-to-run variations of integrated beam current were of the order of a few percent. The obtained normalization factor has been checked with results estimated from the standard target-weight and solid angle measurements.

### B. Experimental results

Figure 1 shows a typical deuteron energy spectrum from the $^{40}$Ca$(p,d)$ reaction in the excitation energy region of 0–10 MeV at 11° laboratory angle. The overall energy resolution was 25–30 keV, which was due mainly to the energy-loss effect in the target.

In the excitation energy region below 5 MeV, almost all the excited states are known from previous work. A group of weakly excited states at $E_x=3.5$–$4.5$ MeV may arise from the coupling of a neutron hole to the collective $3^-$ state at 3.73 MeV in $^{40}$Ca. Thus the effect of two-step processes may be estimated from the strengths of these states. They are relatively weak in comparison with the data at lower bombarding energy [8].

Discrete levels are distributed throughout the excitation energy region below 10 MeV. Four strongly excited states are found at excitation energies below 5 MeV, and several strongly and weakly excited discrete states are found in the excitation energy region $E_x\simeq 5$–10 MeV.

The spectrum data were analyzed with a peak fitting and peeling-off program FOGRAS [9], which provided better data reduction for the complex peak spectra at the higher excitation energy region.

Weak physical backgrounds were subtracted in the excitation energy region of 8–10 MeV. Angular distribution data for typical excited states are shown in Fig. 2. The transitions for the ground (2.463, 2.791, and 3.021 MeV) states have been previously assigned to be $l=2$, $j=\frac{3}{2}$ $(1d_{3/2}^{-1})$, $l=0$, $j=\frac{1}{2}$ $(2s_{1/2}^{-1})$, $l=3$, $j=\frac{7}{2}$ $(1f_{7/2}^{-1})$, and $l=1$, $j=\frac{3}{2}$ $(2p_{3/2}^{-1})$ states, respectively [8]. The 5.128 MeV state has been assigned tentatively to be an $l=2$, $j=\frac{5}{2}$ $(1d_{5/2}^{-1})$ state [8]. This $j$ assignment may be an assumed result from the $l$-$s$ splitting energy of the $1d_{3/2}$ and $1d_{5/2}$ orbits. From the shape of the present analyzing power data, the transferred $l,j$ values are definitely assigned as is understood from the figures. Eighty peaks were analyzed in the excitation energy region of 0–9.5 MeV. The angular distributions of some strongly excited states are shown in Figs. 3–5, together with the distorted-wave Born approximation (DWBA) predictions mentioned below. The experimental results are tabulated in Table I together with the results of Ref. [8] and the energy levels compiled in the Table of isotopes (Table I).

## III. DATA ANALYSIS

The differential cross section and analyzing power data are analyzed with the distorted-wave Born approximation (DWBA) code DWUCK [10] under the zero-range local energy approximation model. It has been known that the conventional calculation with best-fit optical potentials in the proton and deuteron channels does not reproduce the shape of differential cross-section data well for $(p,d)$ reactions at medium energies, and the use of an adiabatic potential for the deuteron channel considerably improves the overall fitting of the angular distribution [11]. For protons, the global optical potential parameters of Menet *et al.* [6], and for deuterons, an adiabatic potential [11] constructed with the proton and neutron optical potential parameters of Becchetti and Greenlees [12], were used. The potential has a standard form,

TABLE I. Spectroscopic results from the $^{40}Ca(p,d)^{39}Ca$ reaction.

| | Present work | | | | Reference [8] | | | | Table of isotopes | |
|---|---|---|---|---|---|---|---|---|---|---|
| No. | $E_x$ (MeV) | $l$ | $J^\pi$ | $C^2S$ | $E_x$ (MeV) | $l$ | $J^\pi$ | $C^2S$ | $E_x$ (MeV) | $J^\pi$ |
| 1 | 0 | 2 | $\frac{3}{2}^+$ | 3.74±0.20[a] | 0 | 2 | $\frac{3}{2}^+$ | 4.2 | 0 | $\frac{3}{2}^+$ |
| 2 | 2.463 | 0 | $\frac{1}{2}^+$ | 1.64±0.15[a] | 2.47 | 0 | $\frac{1}{2}^+$ | 1.9 | 2.467 | $\frac{1}{2}^+$ |
| 3 | 2.791 | 3 | $\frac{7}{2}^-$ | 0.14 | 2.80 | (3) | $\frac{7}{2}^-$ | 0.21 | 2.796 | $\frac{7}{2}^-$ |
| 4 | 3.021 | 1 | $\frac{3}{2}^-$ | 0.01 | 3.03 | 1 | $\frac{3}{2}^-$ | 0.005 | 3.024 | $\frac{3}{2}^-$ |
| 5 | 3.636 | | | | 3.66 | | | | 3.640 | |
| 6 | 3.820 | | | | 3.84 | (3) | $(\frac{5}{2}^-)$ | 0.04 | 3.823 | |
| 7 | 3.886 | | | | | | | | 3.870 | |
| | | | | | | | | | 3.890 | |
| 8 | 3.943 | | | | 3.95 | 1 | $\frac{3}{2}^-$ | 0.006 | 3.936 | |
| | | | | | | | | | 3.951 | |
| 9 | 4.016 | | $\frac{1}{2}^+$ | 0.097 | 4.02 | 0 | $\frac{1}{2}^+$ | 0.09 | 4.021 | $\frac{1}{2}^+$ |
| 10 | 4.340 | 3 | | | 4.32 | | | | | |
| 11 | 4.432 | 2 | $\frac{5}{2}^+$ | 0.033 | 4.43 | | | | | |
| 12 | 4.487 | 3 | $\frac{7}{2}^-$ | 0.01 | 4.49 | (3) | | | | |
| 13 | 4.926 | 2 | $(\frac{5}{2}^+)$ | 0.045 | 4.92 | | | | | |
| 14 | 5.128 | 2 | $\frac{5}{2}^+$ | 1.027 | 5.13 | 2 | $(\frac{5}{2}^+)$ | 1.0 | | |
| 15 | 5.222 | 2 | $\frac{5}{2}^+$ | 0.076 | | | | | | |
| 16 | 5.316 | 3 | $\frac{7}{2}^-$ | 0.02 | | | | | | |
| 17 | 5.364 | | | | 5.34 | (3) | | | | |
| 18 | 5.400 | | | | | | | | | |
| 19 | 5.484 | 2 | $\frac{5}{2}^+$ | 0.490 | 5.49 | 2 | $(\frac{5}{2}^+)$ | 0.45 | | |
| 20 | 5.588 | 2 | $(\frac{5}{2}^+)$ | 0.033 | | | | | | |
| 21 | 5.673 | 2 | $(\frac{5}{2}^+)$ | 0.016 | | | | | | |
| 22 | 5.720 | (3) | $(\frac{7}{2}^-)$ | 0.01 | | | | | | |
| 23 | 5.790 | 1 | $\frac{3}{2}^-$ | 0.01 | 5.75 | | | | | |
| 24 | 5.851 | 1 | $\frac{3}{2}^-$ | 0.002 | | | | | | |
| 25 | 6.009 | (3) | $(\frac{7}{2}^-)$ | 0.03 | 6.01 | | | | | |
| 26 | 6.094 | (0) | $(\frac{1}{2}^+)$ | 0.038 | | | | | | |
| 27 | 6.158 | 2 | $\frac{5}{2}^+$ | 0.940 | 6.15 | 2 | $(\frac{5}{2}^+)$ | 1.1 | | |
| 28 | 6.286 | 2 | $\frac{5}{2}^+$ | 0.044 | | | | | | |
| 29 | 6.405 | 3 | $(\frac{7}{2}^-)$ | 0.03 | 6.40 | | | | | |
| 30 | 6.467 | 2 | $\frac{5}{2}^+$ | 0.079 | | | | | | |
| 31 | 6.514 | 2 | $(\frac{5}{2}^+)$ | 0.038 | | | | | | |
| 32 | 6.580 | 3 | $(\frac{7}{2}^-)$ | 0.01 | 6.57 | | | | | |
| 33 | 6.629 | | | | | | | | | |
| 34 | 6.722 | 3 | $(\frac{7}{2}^-)$ | 0.01 | | | | | | |
| 35 | 6.794 | 2 | $\frac{5}{2}^+$ | 0.056 | 6.79 | (2) | $(\frac{5}{2}^+)$ | 0.04 | | |
| 36 | 6.835 | | | | | | | | | |
| 37 | 6.906 | 0 | $\frac{1}{2}^+$ | 0.01 | 6.90 | | | | | |
| 38 | 6.954 | 3 | | | | | | | | |
| 39 | 7.025 | (3) | $(\frac{5}{2}^-)$ | | | | | | | |
| 40 | 7.060 | | | | | | | | | |
| 41 | 7.132 | 2 | $\frac{5}{2}^+$ | 0.046 | | | | | | |
| 42 | 7.199 | 2 | $\frac{5}{2}^+$ | 0.197 | 7.19 | 2 | $(\frac{5}{2}^+)$ | 0.21 | | |
| 43 | 7.248 | 2 | $\frac{5}{2}^+$ | 0.036 | | | | | | |
| 44 | 7.310 | (3) | | | | | | | | |
| 45 | 7.380 | 2 | $\frac{5}{2}^+$ | 0.121 | 7.34 | 2 | $(\frac{5}{2}^+)$ | 0.10 | | |
| 46 | 7.427 | (2) | $(\frac{5}{2}^+)$ | 0.018 | | | | | | |
| 47 | 7.480 | (3) | | | | | | | | |
| 48 | 7.532 | (3) | | | | | | | | |
| 49 | 7.581 | (3) | | | | | | | | |
| 50 | 7.635 | (3) | | | | | | | | |

TABLE I. (*Continued.*)

| | Present work | | | | Reference [8] | | | | Table isotopes | |
|---|---|---|---|---|---|---|---|---|---|---|
| No. | $E_x$ (MeV) | $l$ | $J^\pi$ | $C^2S$ | $E_x$ (MeV) | $l$ | $J^\pi$ | $C^2S$ | $E_x$ (MeV) | $J^\pi$ |
| 51 | 7.711 | 2 | $\frac{5}{2}^+$ | 0.046 | | | | | | |
| 52 | 7.773 | | | | | | | | | |
| 53 | 7.840 | | | | | | | | | |
| 54 | 7.924 | 2 | $\frac{5}{2}^+$ | 0.104 | 7.92 | 2 | $(\frac{5}{2}^+)$ | 0.33 | | |
| 55 | 7.972 | 2 | $\frac{5}{2}^+$ | 0.231 | | | | | | |
| 56 | 8.021 | 2 | $(\frac{5}{2}^+)$ | 0.041 | | | | | | |
| 57 | 8.082 | 2 | $(\frac{5}{2}^+)$ | 0.031 | | | | | | |
| 58 | 8.157 | 2 | $\frac{5}{2}^+$ | 0.112 | | | | | | |
| 59 | 8.219 | 2 | $\frac{5}{2}^+$ | 0.078 | | | | | | |
| 60 | 8.280 | 2 | $(\frac{5}{2}^+)$ | 0.026 | | | | | | |
| 61 | 8.336 | 2 | $\frac{5}{2}^+$ | 0.142 | 8.31 | | | | | |
| 62 | 8.396 | 2 | $(\frac{5}{2}^+)$ | 0.023 | | | | | | |
| 63 | 8.460 | 2 | $(\frac{5}{2}^+)$ | 0.052 | | | | | | |
| 64 | 8.509 | 2 | $\frac{5}{2}^+$ | 0.071 | | | | | | |
| 65 | 8.582 | 2 | $(\frac{5}{2}^+)$ | 0.035 | | | | | | |
| 66 | 8.650 | 2 | $(\frac{5}{2}^+)$ | 0.019 | | | | | | |
| 67 | 8.692 | 2 | $\frac{5}{2}^+$ | 0.106 | | | | | | |
| 68 | 8.748 | 2 | $(\frac{5}{2}^+)$ | 0.025 | | | | | | |
| 69 | 8.806 | 2 | $(\frac{5}{2}^+)$ | 0.030 | | | | | | |
| 70 | 8.895 | | | | | | | | | |
| 71 | 8.937 | 2 | $\frac{5}{2}^+$ | 0.032 | | | | | | |
| 72 | 8.988 | 2 | $\frac{5}{2}^+$ | 0.038 | | | | | | |
| 73 | 9.039 | 2 | $\frac{5}{2}^+$ | 0.052 | | | | | | |
| 74 | 9.104 | 2 | $(\frac{5}{2}^+)$ | 0.017 | | | | | | |
| 75 | 9.158 | 2 | $\frac{5}{2}^+$ | 0.037 | | | | | | |
| 76 | 9.213 | 2 | $(\frac{5}{2}^+)$ | 0.026 | | | | | | |
| 77 | 9.271 | | | | | | | | | |
| 78 | 9.329 | | | | | | | | | |
| 79 | 9.426 | | | | | | | | | |
| 80 | 9.505 | | | | | | | | | |

[a]The errors are due to the ambiguity in fitting the theoretical to experimental angular distributions. The absolute normalization measurement error is not included because of the renormalization procedure used for the neutron bound-state calculations in the DWBA analysis.

$$V(r)=V_C(r_c)-V(e^x+1)^{-1}$$
$$-i\left[W-4W_D a'\frac{d}{dr}\right](e^{x'}+1)^{-1}$$
$$+\left[\frac{\hbar}{m_\pi c}\right]^2 V_{so}\frac{1}{r}\frac{d}{dr}(e^{x''}+1)^{-1}\sigma I\ , \qquad (1)$$

where $x=(r-R_0)/a_0$, $x'=(r-R')/a'$, $x''=(r-R'')/a''$ with $R_0=r_0A^{1/3}$, etc., and the Coulomb potential $V_C$ is that for a uniformly charged sphere of radius $R_C=r_CA^{1/3}$.

Menet *et al.*'s potential parameters [6] for protons are given by

$$V=49.9-0.22E+26.4(N-Z)/A+0.4Z/A^{1/3}\ \text{MeV}\ ,$$
$$r_0=1.16\ \text{fm}\ ,\quad a_0=0.75\ \text{fm}\ ,$$
$$W=1.2+0.09E\ (\text{MeV})\ ,$$
$$W_D=4.2-0.05E+15.5(N-Z)/A\ \text{or}\ 0\ \text{MeV}\ ,$$
whichever is greater , (2)
$$r'=1.37\ \text{fm}\ ,$$
$$a'=0.74-0.0008E+1.0(N-Z)/A\ \text{fm}\ ,$$
$$V_{so}=6.04\ \text{MeV}\ ,\quad r''=1.064\ \text{fm}\ ,\quad a''=0.78\ \text{fm}\ ,$$
$$r_C=1.25\ \text{fm}\ .$$

The constructed adiabatic potential parameters for deuterons are given by

$$V=110.3-0.65(E/2)+0.4Z/A^{1/3}\ \text{MeV}\ ,$$

$$r_0=1.17\ \text{fm}\ ,\quad a_0=0.779\ \text{fm}\ ,$$

$$W=0.44(E/2)-4.26\ \text{or}\ 0\ \text{MeV}\ ,$$

whichever is greater ,

$$W_D=24.8-0.50(E/2)\ \text{or}\ 0\ \text{MeV}\ ,$$

whichever is greater , (3)

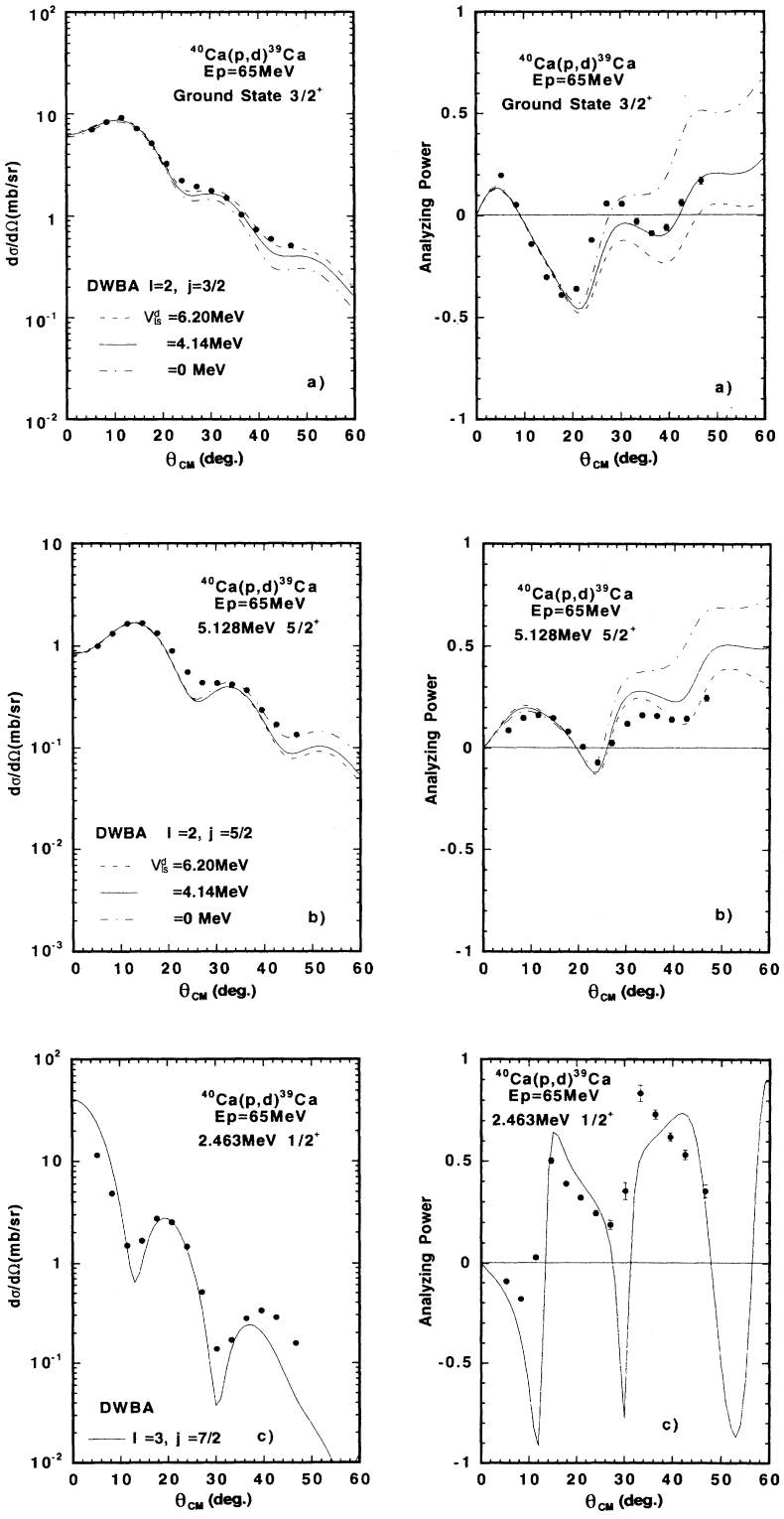


FIG. 2. Angular distribution data of cross sections (left) and analyzing powers (right) for typical single hole states: (a) the ground $\frac{3}{2}^+$ ($l=2$, $j=\frac{3}{2}$) state, (b) the 5.128 MeV $\frac{5}{2}^+$ ($l=2$, $j=\frac{5}{2}$) state, (c) the 2.463 MeV $\frac{1}{2}^+$ ($l=0$, $j=\frac{1}{2}$) state, (d) the 2.791 MeV $\frac{7}{2}^-$ ($l=3$, $j=\frac{7}{2}$) state, and (e) the 3.021 MeV $\frac{3}{2}^-$ ($l=1$, $j=\frac{3}{2}$) state, in $^{39}Ca$. The curves show predictions of the DWBA theory.

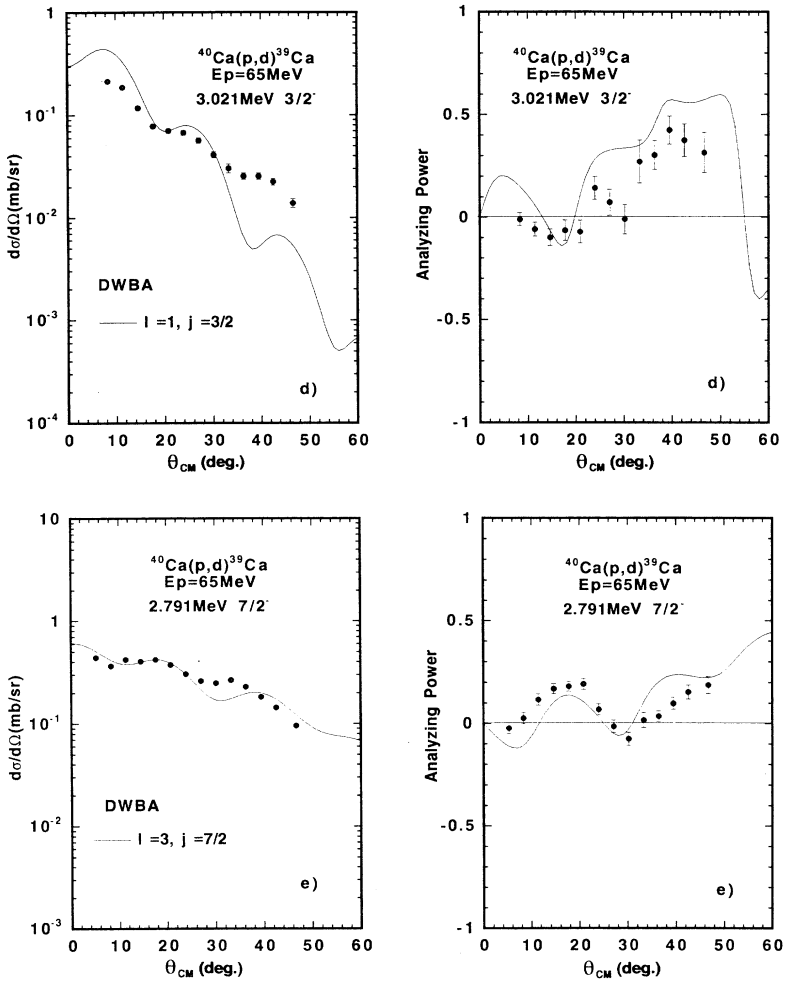


FIG. 2. (*Continued*).

$r'=1.29$ fm , $a'=0.578+0.35(N-Z)/A$ fm ,

$V_{so}=6.2$ MeV , $r''=1.06$ fm , $a''=0.75$ fm ,

$r_C=1.25$ fm .

The prescription of the adiabatic deuteron potential is given by Satchler [13]. In the original paper, it is suggested to modify the real and imaginary potential depths in order to keep constant the volume integrals. Since however, the change of DWBA results with these modifications is small, they are neglected here. The calculation with these potentials reasonably reproduces the differential cross-section data, but not the analyzing power data. A reduction of the depth of the spin-orbit potential improves the fitting considerably as shown in Fig. 2 and does not largely change the shape of the differential cross section. Then, the reduced depth of $\frac{2}{3}$ ($\sim$4 MeV) is used in the following analysis.

The neutron bound-state wave function is calculated generally with the separation energy method or the effective binding energy method. These two methods calculate the wave function of the pickup neutron bound in a Woods-Saxon well with a searched potential depth to asymptotically give the input binding energy. The latter method has been preferred for the analysis of one nucleon transfer reactions in a wide excitation energy region. Recently, the bound-state wave function has been calculated with the addition of a peak at the surface of the Woods-Saxon potential to take into account the residual interaction [14,15] (the surface peak method). Since this method has little effect on the sum of the resultant spectroscopic factors, the conventional effective binding energy method is adopted in the present work. Typical results of calculations for different $l,j$ transfers are shown in Figs. 2–5. The DWBA theory reasonably reproduces the experimental data. The bound-state parameters have significant influence on the absolute normalization of the calculated differential cross section. The Woods-Saxon parameters $r_0,a_0$ for the neutron bound state have been adjusted in this work [3] to yield expected summed occupation numbers for the neutron $1f_{7/2}$, $2s_{1/2}$, and $1d_{3/2}$ shells (total neutron number $\simeq 6$) in the $^{40}$Ca nucleus, giving $r_0=1.27$ fm and $a_0=0.70$ fm with 25 times the spin-orbit Thomas term. In the local energy approximation calculation of DWBA, the parameter of the finite range effect, 0.629 is used. And parameters of the nonlocality

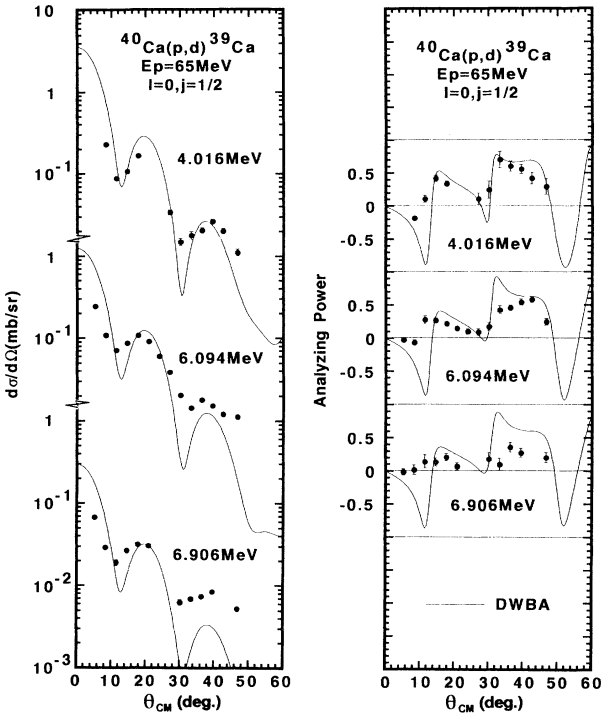


FIG. 3. Angular distribution data of cross sections (left) and analyzing powers (right) for some $\frac{1}{2}^+$ ($l=0$, $j=\frac{1}{2}$) states in $^{39}$Ca.

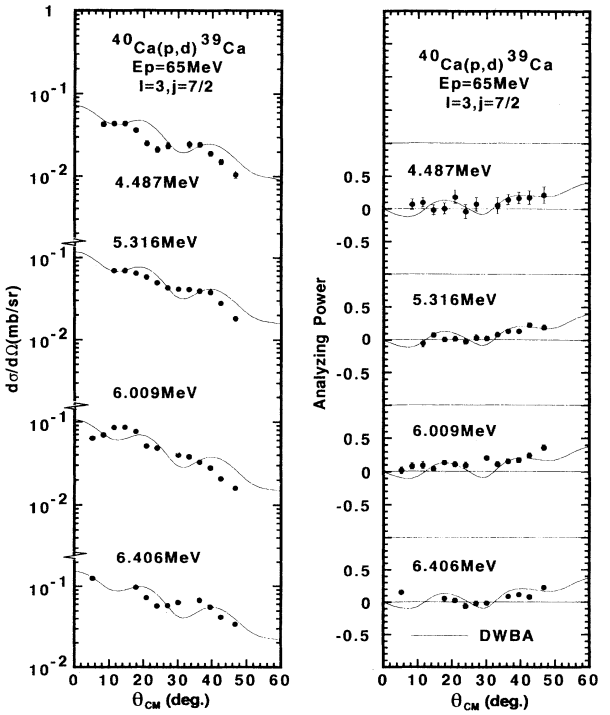


FIG. 4. Angular distribution data of cross sections (left) and analyzing powers (right) for some $\frac{7}{2}^-$ ($l=3$, $j=\frac{7}{2}$) states in $^{39}$Ca.

effects for neutron, proton, and deuteron potentials, $\beta_n=0.85$, $\beta_p=0.85$, and $\beta_d=0.54$, respectively, are adopted.

The spectroscopic factor for a $(p,d)$ reaction for $j$ transfer can be obtained with

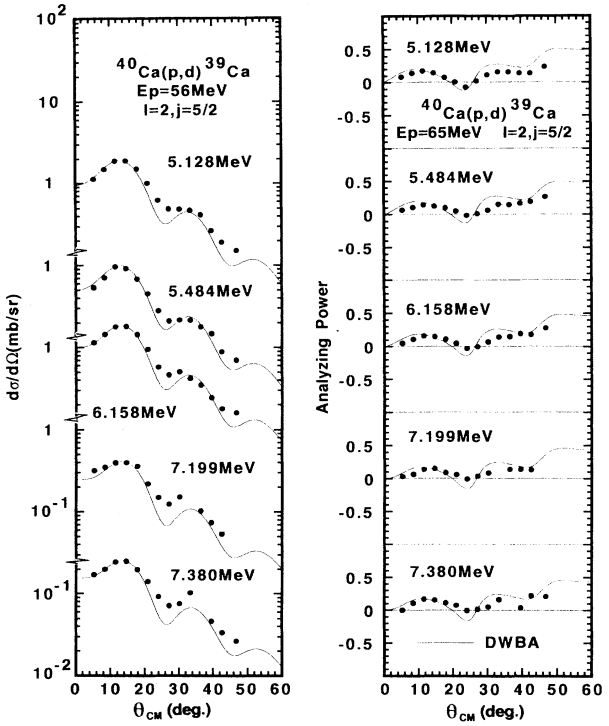


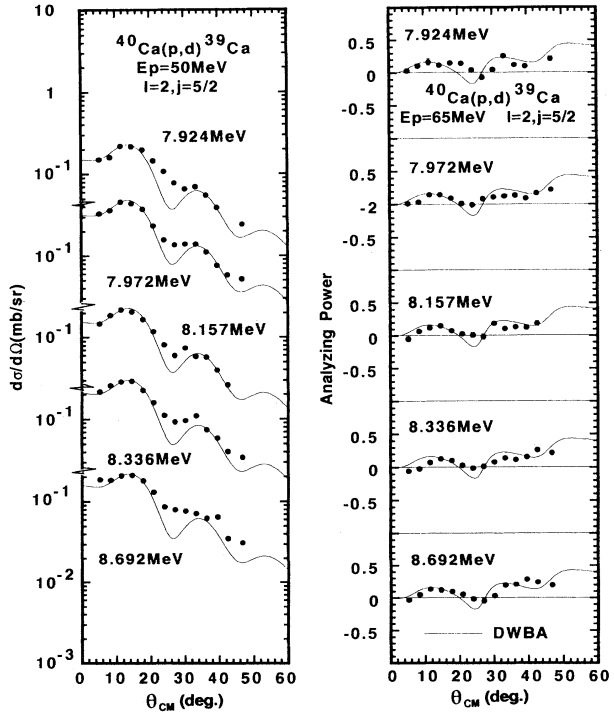


FIG. 5. Angular distribution data of cross sections (left) and analyzing powers (right) for some $\frac{5}{2}^+$ ($l=2$, $j=\frac{5}{2}$) states in $^{39}$Ca.

$$\frac{d\sigma}{d\Omega}=2.30\frac{C^2S}{2j+1}\frac{d\sigma}{d\Omega}\bigg|_{\text{DWUCK}}, \quad (4)$$

where $C^2S$ is the spectroscopic factor for the transition and $d\sigma/d\Omega|_{\text{DWUCK}}$ the resultant DWBA differential cross section with the code DWUCK [10].

From comparisons between experiment and theory, the transferred angular momenta $l,j$ are assigned, the spectroscopic factors are determined for 58 peaks in the excitation energy region from 0 to about 9.5 MeV, and the results are tabulated in Table I. For almost all the strongly excited states, the diffraction patterns are clear to assign the $l,j$ values. It is, however, difficult to assign transferred angular momenta for some excited states near the excitation energy of about 3.5–4.5 MeV, which may arise from coupling of a neutron hole to the 3.72 MeV $3^-$ state in the $^{40}$Ca core, as mentioned before. It is also difficult to assign the $l,j$ values to some weakly excited states in the excitation energy region of 5–10 MeV. The strengths of these levels are considerably weaker at the incident energy of 65 MeV than in lower-energy experiments.

## IV. DISCUSSIONS

### A. Single hole states

The present results supply information mainly on shell occupations in the $1d_{5/2}$, $1d_{3/2}$, $2s_{1/2}$, and $1f_{7/2}$ orbits in $^{39}$Ca. It is noted first that the fragmentation of the hole strengths of two surface orbits, $1d_{3/2}$ and $2s_{1/2}$, is weak. In particular, the $1d_{3/2}$ hole strength is rarely found in the excitation energy region of 0–10 MeV, except in the ground state.

In estimating the shell occupation probabilities of the observed shell orbits, the normalization procedure of the DWBA calculation is important. The absolute value of the spectroscopic factor changes largely with the bound-state parameters of the pickup neutron. In the present work, the bound-state parameters are determined to keep the number of surface neutrons to be about six for the $1d_{3/2}$, $2s_{1/2}$, and $1f_{7/2}$ shells combined in the $^{40}$Ca nucleus, as described in the previous section. With this condition, the fullness amplitudes of the $1d_{3/2}$ and $2s_{1/2}$ hole states are 85–90%. Considerable defects of particles in the surface shell orbits may arise from the two-particle–two-hole correlation in the $^{40}$Ca ground state [16]. The occupation probabilities of $1d_{5/2}$, $1d_{3/2}$, $2s_{1/2}$, $1f_{7/2}$, and $2p_{3/2}$ shells are determined from the obtained spectroscopic factors, and the results are shown in Table II together with the predictions of some theoretical models. In the summation process of the spectroscopic factors, some data for which the assignments of transferred $j$ values are ambiguous (in parentheses) are included, because the effects on the final results are small. The experimental surface softness of $^{40}$Ca is in good agreement with those from the BCS calculation and from the second random-phase-approximation (RPA) calculation [16]. It is reasonable to use second RPA results for investigating the mechanism of highly excited states, for example, Gamow-Teller and $M1$ giant resonances. It is noted that recent results [17,18] from mean-field calculations suggest more depletion in deep shell orbits.

TABLE II. Occupation probabilities of the shell model orbits in $^{39}$Ca.

| | $(p,d)$[a] | BCS[b] | Second RPA[c] | Mean-field theory[d] |
|---|---|---|---|---|
| $2p_{3/2}$ | 0.01±0.001 | 0.02 | 0.03 | 0.08 |
| $1f_{7/2}$ | 0.03±0.003 | 0.04 | 0.06 | 0.12 |
| $1d_{3/2}$ | 0.93±0.05 | 0.86 | 0.89 | 0.88 |
| $2s_{1/2}$ | 0.89±0.08 | 0.94 | 0.92 | 0.89 |
| $1d_{5/2}$ | >0.79[e] | 0.99 | 0.93 | 0.90 |

[a]Present work. The errors are estimated from those of the spectroscopic factors. Errors in the constraint from the renormalization procedure in the DWBA analysis are not included. See text.
[b]$G=20/A$ and single-particle energies of Johnson and Mahaux.[17]
[c]Nishizaki *et al.*, Ref. [16].
[d]Table 5, line 8 in Ref. [18].
[e]Missing strengths may exist in higher excitation energy.

For the 2.79 MeV $\frac{7}{2}^-$ state, the obtained spectroscopic factor is 0.14, which is quite a bit smaller than those from experiments at lower bombarding energies, for example, 0.25–0.35 at 27.5 MeV [19] and 0.21 at 40 MeV [8]. Since the value of the spectroscopic factors for other single hole states does not change largely in this energy range, this result may suggest the existence of two-step process and/or the effect of the reaction form factor for weak particle states.

The $l=2$ strength distributed in the 5–10 MeV excitation energy region arises almost exclusively from the $l=2$, $j=\frac{5}{2}$ $(1d_{5/2}^{-1})$ transfer, and this excitation corresponds to that of a deeply bound hole state. The strength of deeply bound hole states is distributed frequently in two separated parts, a few strongly excited states near the lower excitation energy region and a group of weakly excited states at the center region of the fragmentation. This fact has been predicted theoretically and confirmed qualitatively by experimental bump spectra of deeply bound hole states, and is confirmed in the present data obtained by peak-by-peak analysis with unambiguous $l,j$ assignments from polarized beam experiments. This result also suggests an origin of the fragmentation of $6^-(1f_{7/2}, 1d_{5/2}^{-1})$ stretched states excited through the $^{40}$Ca$(p,n)^{40}$Sc reaction, i.e., the fragmentation of $1d_{5/2}$ hole strength [3].

### B. Spreading width of the hole states

The spreading (damping) width of the single particle or hole states provides a good measure to understand the excitation mechanism of highly excited states [20]. The widths had been given at first by full widths at half maximum (FWHM) in the obtained strength functions. The spreading width should be estimated principally by fitting a Lorentzian shape to the strength function if the interaction matrix elements and the level densities do not change

over the analyzed energy region. However, the level density in fact changes significantly in the excitation energy region where deeply bound hole states are observed. In the last decade, the strength functions have been determined for deeply bound hole states in some cases, and the widths estimated from the second moment of the strength function [20]:

$$\Gamma_{\downarrow}=2.35\sigma ,$$
$$\sigma^2=\frac{\sum(E_x-\bar{E}_x)^2C^2S_j(E_x)}{\sum C^2S_j(E_x)} \quad (5)$$

and

$$\bar{E}_x=\frac{\sum E_xC^2S_j(E_x)}{\sum C^2S_j(E_x)} ,$$

where $C^2S_j(E_x)$ is the strength function for the $j$ hole state as a function of the excitation energy $E_x$. If the experimental and theoretical widths are estimated using the same procedure, the comparison and discussion may be internally consistent. Table III summarizes the obtained spreading widths of $1d_{3/2}$, $2s_{1/2}$, and $1d_{5/2}$ hole states together with the total spectroscopic factors and the average excitation energies. Errors may arise in the deduced spreading width from the effects of the missing strengths of states at an excitation energy far from the average energy, the subtraction of the physical background and the uncertainty in the DWBA analysis. We have not estimated them because the interrelationships among the various contributions are too difficult to disentangle. The spreading widths are also plotted in Fig. 6 as a function of energy measured from the corresponding Fermi surface ($E-E_F$), together with some previous results.[21–23] The Fermi energy is calculated with the procedure based on the work by Jeukenne, Mahaux, and Sartor [24]:

$$E_F=(E_{F\tau^-}+F_{F\tau^+})/2 ,$$
$$E_{F\tau^-}=(M_A-M_{A-1}-m_\tau)C^2 , \quad (6)$$
$$E_{F\tau^+}=(M_{A+1}-M_A-m_\tau)C^2 ,$$

TABLE III. Summations of spectroscopic factors, average excitation energies and spreading widths from the present results ($E_x$=0–9.5 MeV).

| Orbit | $\sum C^2S$ | $E$ (MeV) | $\Gamma$ (MeV) |
|---|---|---|---|
| $1d_{3/2}^{-1}$ | 3.74 | 0 | 0 |
| $2s_{1/2}^{-1}$ | 1.79 | 2.65 | 1.64 |
| $1d_{5/2}^{-1}$ | 4.72 | 6.61 | 3.17 |

where $M_A$ is the mass of nucleus $A$, while $m_\tau$ denotes the mass of a proton ($\tau=p$) or of a neutron ($\tau=n$). In the independent particle model, $E_{F^-}$ is identified with the energy of the "last" (least bound) occupied orbit and $E_{F^+}$ with that of the "first" (most bound) unoccupied orbit. Jeukenne, Mahaux, and Sartor have generated a compilation of the Fermi energy for neutrons and protons in nuclei with mass numbers $40\leq A\leq 208$ [24] using Eq. (6). In the experimental mass value, however, higher nuclear structure effects (for example, the shell, pairing, and collective effects) are naturally included and the selection of data may affect the final results. We adopted the values calculated from a mass formula neglecting shell and pairing effects and obtained relations as follows [25]:

$$E_{Fn}=-12.20+33.81\eta \text{ MeV} ,$$
$$E_{Fp}=-12.16-37.55\eta-83.25\eta^2+\Delta E_C(A,Z) \text{ MeV} , \quad (7)$$

where $\eta$ is the symmetry parameter, $(N-Z)/A$, and $\Delta E_C(A,Z)$ is the Coulomb energy difference (in MeV),

$$0.717[Z^2/A^{1/3}-(Z-1)^2/(A-1)^{1/3}]$$
$$-1.211[Z^2/A-(Z-1)^2/(A-1)] .$$

It should be noted that the resultant width of the $1d_{3/2}$ hole state is equal to zero because no excited $\frac{3}{2}^+$ states can be found in the excitation energy region 0–10 MeV. The experimental data in Fig. 6 are distributed smoothly as a function of energy, except for the $^{39}$Ca case, which is rather consistent with that in the doubly closed shell nucleus $^{208}$Pb cited in Ref. [20]. In Fig. 6, the dashed line

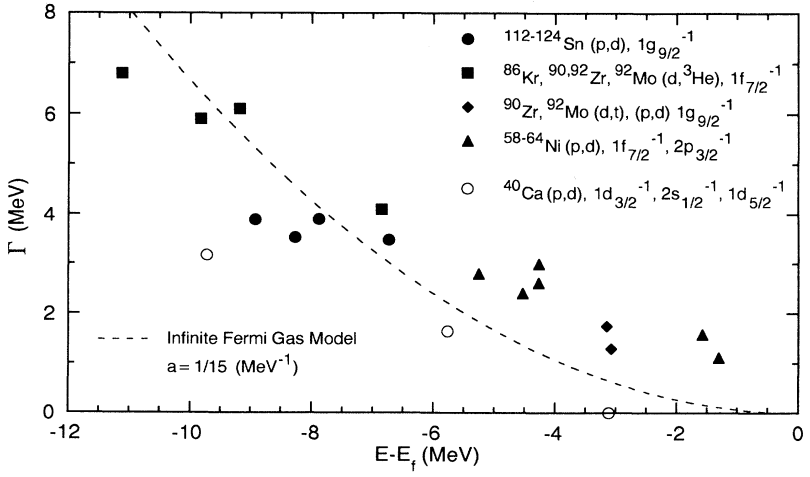


FIG. 6. Spreading widths determined from the strength functions obtained with nucleon pickup reactions on medium weight nuclei. Open circles show results in the present work. Solid circles, triangles, and squares show previous results [19,21–23]. Dashed line shows a prediction of the infinite Fermi particle model with $a=\frac{1}{15}$ MeV$^{-1}$.

shows the energy dependence predicted by the infinite Fermi gas model:

$$\Gamma_{\downarrow}=a(E-E_F)^2 , \quad a=\tfrac{1}{15}\ \mathrm{MeV}^{-1} . \tag{8}$$

Pfeifer *et al.* [26] obtained the widths of $1f_{7/2}$ proton hole states from $(d,{}^3\mathrm{He})$ reactions on nuclei in the mass region $^{88}$Sr-$^{92}$Mo, with results that agree well with the estimation from the above prediction. However, the theoretical prediction by Bertsch *et al.* with the single-particle doorway model for the $^{208}\mathrm{Pb}+n$ system shows a rather sudden onset of damping at 4–5 MeV and a plateau in the energy region of 5–10 MeV, and this trend agrees with a few experimental data cited in their original paper [27]. The present data agree qualitatively with the prediction of Bertsch *et al.*, although this comparison is not exact for the present $^{40}\mathrm{Ca}+n$-hole case.

It is known that the spreading width is related to the imaginary part of the single-particle potential based on the dispersion relation of the optical model [18,28,29]. The present data provide more accurate information on the potential near the Fermi surface [21].

## V. CONCLUSION

Cross sections and analyzing powers for the $^{40}\mathrm{Ca}(p,d)$ reaction to 80 excited states of $^{39}$Ca have been measured with a polarized proton beam at 65 MeV incident energy. The data were analyzed to determine the transferred angular momenta $l,j$ and the spectroscopic factors for the 58 transitions mainly to the $1d_{3/2}$, $2s_{1/2}$, and $1d_{5/2}$ single hole states. The deduced occupation probabilities agree fairly well with the prediction of a second RPA ground-state correlation calculation in the surface shells of $^{40}$Ca. The spreading widths were determined from the distribution of the spectroscopic factors.

## ACKNOWLEDGMENTS

We are grateful to Professor H. Ikegami and the staff of the Research Center for Nuclear Physics (RCNP), Osaka University, for the support of the experiments at the cyclotron facility. This work was performed at the RCNP under Program Nos. 30A08 and 31A08.

[1] T. Chittrakarn, B. D. Anderson, A. R. Baldwin, C. Lebo, R. Madsey, and S. W. Watson, Phys. Rev. C **34**, 80 (1986).
[2] J. Källne and B. Fagerström, Phys. Scr. **11**, 79 (1975).
[3] M. Matoba, H. Ijiri, H. Ohgaki, S. Uehara, T. Fujiki, Y. Uozumi, H. Kugimiya, N. Koori, I. Kumabe, and M. Nakano, Phys. Rev. C **39**, 1658 (1989).
[4] H. Ikegami, S. Morinobu, I. Katayama, M. Fujiwara, and S. Yamabe, Nucl. Instrum. Methods **175**, 33 (1980).
[5] M. Matoba, K. Tsuji, K. Marubayashi, T. Shintake, H. Ikegami, T. Yamazaki, S. Morinobu, I. Katayama, M. Fujiwara, and Y. Fujita, Nucl. Instrum. Methods **180**, 419 (1981).
[6] J. J. H. Menet *et al.*, Phys. Rev. C **4**, 1114 (1971).
[7] C. B. Fulmer, J. B. Ball, A. Scott, and M. L. Whiten, Phys. Rev. **181**, 1113 (1969).
[8] P. Martin, M. Buenerd, Y. Dupont, and M. Chabre, Nucl. Phys. **A185**, 465 (1972).
[9] S. Matsuki, code FOGRAS, Kyoto University, Chemical Research Institute (unpublished).
[10] P. D. Kunz, code DWUCK, University of Colorado (unpublished).
[11] R. C. Johnson and P. J. R. Soper, Phys. Rev. C **1**, 976 (1970).
[12] F. P. Becchetti, Jr. and G. W. Greenlees, Phys. Rev. **182**, 1190 (1969).
[13] G. R. Satchler, Phys. Rev. C **4**, 1485 (1971).
[14] G. L. Wales and R. C. Johnson, Nucl. Phys. **A274**, 168 (1976).
[15] N. Austern, Nucl. Phys. **A292**, 190 (1977); W. D. M. Res, Ph.D. thesis, Oxford University, 1976 (unpublished).
[16] S. Nishizaki, S. Drożdż, J. Wambach, and J. Speth, Phys. Lett. B **215**, 231 (1988).
[17] C. H. Johnson and C. Mahaux, Phys. Rev. C **38**, 2589 (1988).
[18] C. Mahaux and R. Sartor, Nucl. Phys. **A528**, 253 (1991).
[19] R. J. Philpott, W. T. Pinkston, and G. R. Satchler, Nucl. Phys. **A119**, 241 (1968).
[20] G. F. Bertsch, P. F. Bortignon, and R. A. Broglia, Rev. Mod. Phys. **55**, 287 (1983).
[21] M. Matoba, T. Sakae, Y. Uozumi, O. Iwamoto, K. Hisamochi, H. Ijiri, Y. Watanabe, N. Koori, T. Maki, and M. Nakano, J. Phys. Soc. Jpn. **61**, 3827 (1992); (unpublished).
[22] M. Matoba, H. Ijiri, H. Kametani, I. Kumabe, M. Hyakutake, N. Koori, T. Sakae, and T. Maki, Nucl. Phys. **A456**, 235 (1986).
[23] N. Matsuoka *et al.*, RCNP Osaka University (private communications).
[24] J. P. Jeukenne, C. Mahaux, and R. Sartor, Phys. Rev. C **43**, 2211 (1991).
[25] K. Hisamochi *et al.*, Kyushu University (private communication).
[26] A. Pfeifer, G. Mairle, K. T. Knöphle, T. Kihm, G. Seegert, P. Granbmayr, G. J. Wagner, V. Bechtold, and L. Friedrich, Nucl. Phys. **A455**, 381 (1986).
[27] G. F. Bertsch, P. F. Bortignon, R. A. Broglia, and CH. Dasso, Phys. Lett. **80B**, 161 (1979).
[28] C. Mahaux and H. Ngô, Phys. Lett. **100B**, 285 (1981).
[29] C. Mahaux and R. Sartor, Nucl. Phys. **A484**, 205 (1988).